Sustainable Ultra High-Performance Geopolymer Composite

Jian-Guo Dai[1], Surendra P. Shah[2]

[1]*Professor, Department of Civil and Environmental Engineering, Honk Kong Polytechnic University, Hong Kong, China*
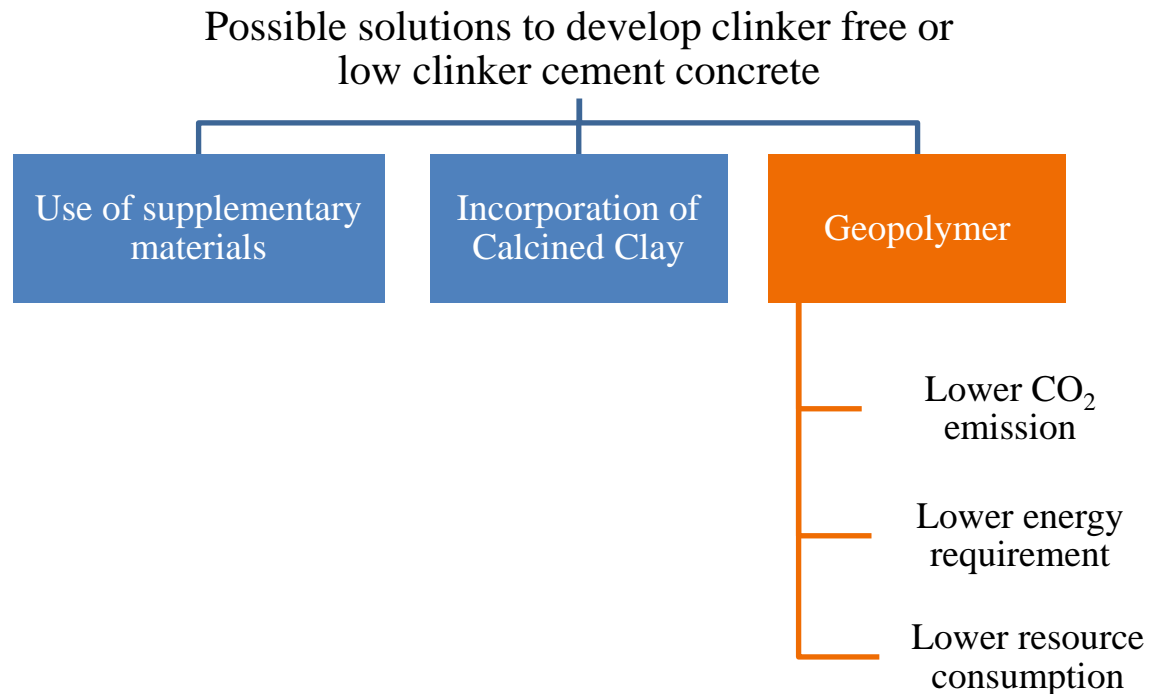*cejgdai@polyu.edu.hk*

[2]*Professor, Department of Civil Engineering and Materials Science and Engineering, Director, Center for Advanced Construction Materials, UTA, USA*
surendra,shah@uta.edu

ACI Spring 2023
Nanotechnology for Concrete with Low Carbon Footprint
April 2 - 6, 2023, Hilton San Francisco Union Square, San Francisco, CA

How to reduce clinker content?

- Portland cement production contributes 5-7% of the global carbon emissions.

- Almost 1 kg of CO_2 is released for 1kg of cement produced from the decomposition of calcium carbonate and the burning of fossil fuel.

Possible solutions to develop clinker free or low clinker cement concrete

Use of supplementary materials	Incorporation of Calcined Clay	Geopolymer

- Lower CO_2 emission
- Lower energy requirement
- Lower resource consumption

What is geopolymer?

The term 'geopolymer' was first applied to the products of alkaline activation of calcined clays (particularly metakaolin) by Davidovits in the 1970s.

Geopolymer is an alkali-activated binder material containing little or no calcium; often derived from a metakaolin or a fly ash precursor.
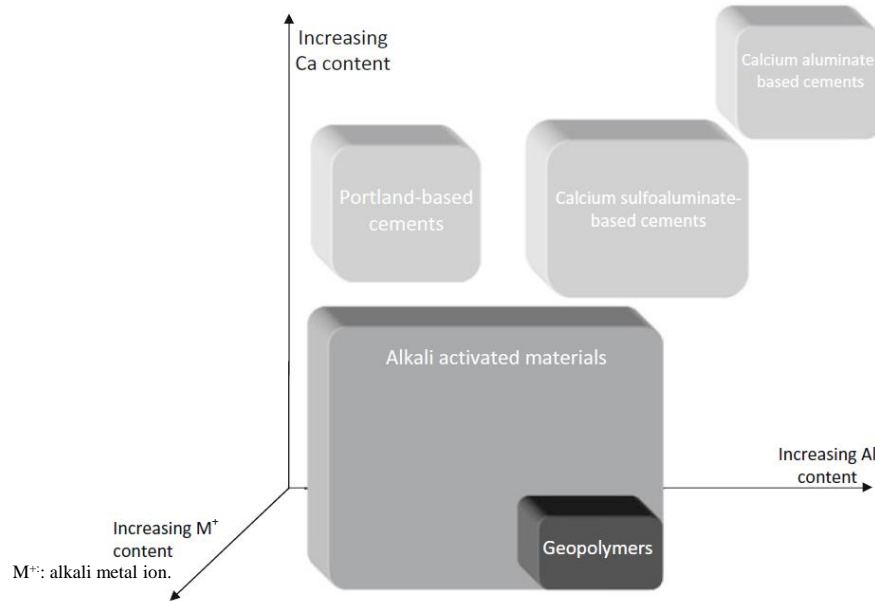
Shading indicates approximate alkali content; darker shading corresponds to higher concentrations of Na and/or K

Reaction chemistry:

Solid alkali-activator

(e.g. NaOH, Na_2SiO_3 etc.)

+

Aluminosilicate precursor
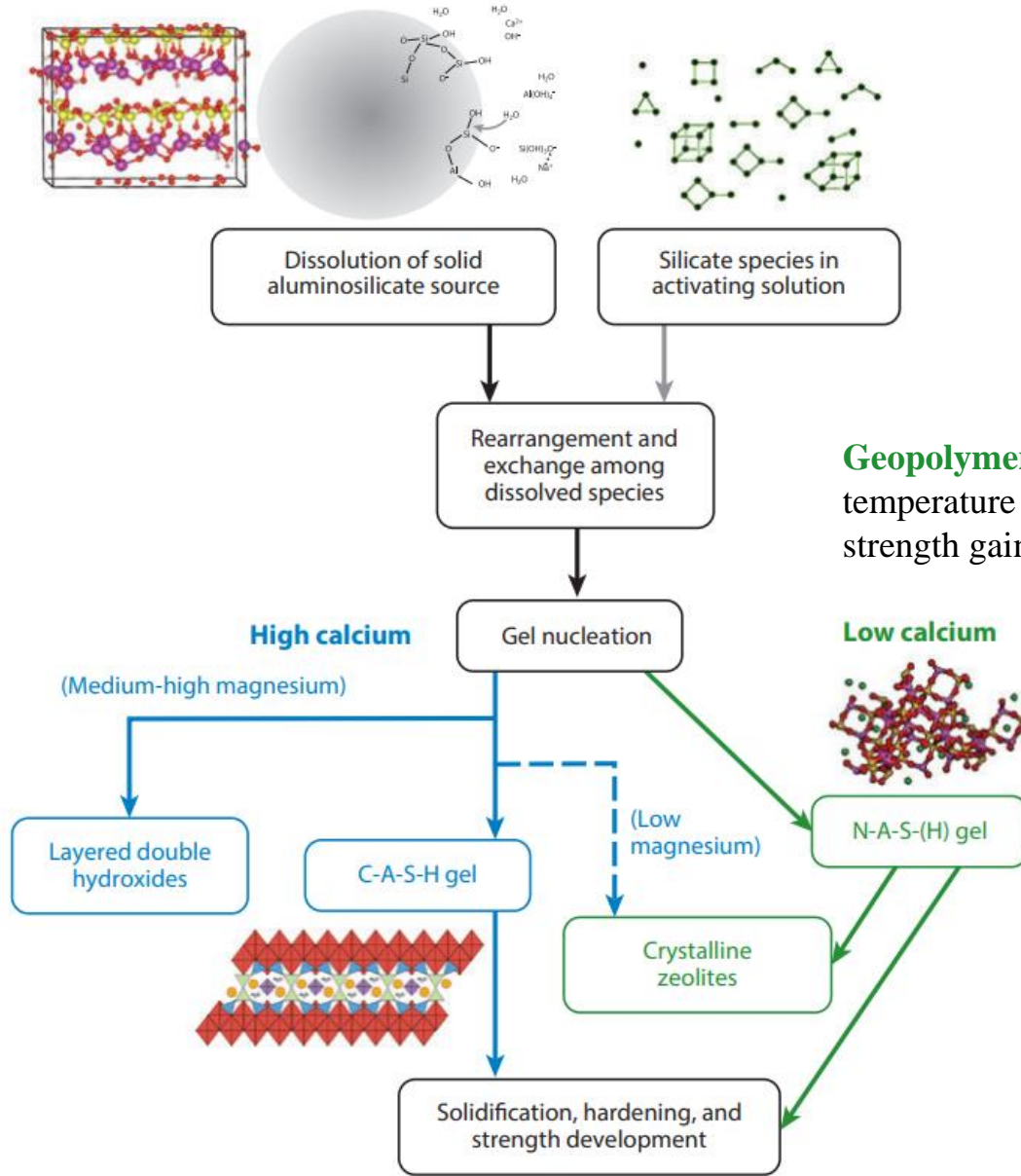
=

Alkali Activated Material

Reaction mechanism and properties are different for:
- High Calcium Alkali Activated Materials
- Low Calcium Alkali Activated Materials

Provis, John L., and Jannie SJ Van Deventer, eds. *Alkali activated materials, RILEM* (2013).

UNIVERSITY OF TEXAS ARLINGTON

Reaction Mechanism

Dissolution of solid aluminosilicate source

Silicate species in activating solution

Rearrangement and exchange among dissolved species

Geopolymers often requires high temperature curing for adequate strength gain

High calcium

(Medium-high magnesium)

Gel nucleation

Low calcium

Layered double hydroxides

C-A-S-H gel

(Low magnesium)

N-A-S-(H) gel

Crystalline zeolites

Solidification, hardening, and strength development

Provis, John L., and Susan A. Bernal. *Annual Review of Materials Research* 44 (2014): 299-327.

UHPC with steel fibers

Chemical components and loss on ignition (LOI) values of precursors obtained using XRF

Chemical composition	FA	GGBS	SF
Aluminum oxide	25.80	14.10	0.15
Silicon oxide	52.40	32.10	96.90
Calcium oxide	6.42	44.20	0.53
Ferric oxide	8.40	0.32	0.06
Magnesium oxide	2.27	5.95	1.10
Sulfur trioxide	0.86	1.74	0.12
Titanium dioxide	1.31	0.66	-
Phosphorus oxide	0.66	0.12	0.33
Potassium oxide	1.47	0.42	0.78
Others	0.41	0.39	0.03
LOI (950°C)	3.48	0.26	1.78

UNIVERSITY OF TEXAS ARLINGTON

Mix design and curing conditions

Mix Design

Mix ID	Precursors			Fine Sand	Activators		Borax	Extra Water	Fiber content (Vol.)[*]
	FA	GGBS	SF		Na_2SiO_3 – Anhydrous	Waterglass			
F6S4-3%	0.6	0.4	0.084	0.705	0.103	0.153	0.051	0.105	3%
F4S6-3%	0.4	0.6							3%
F2S8-3%	0.2	0.8							3%
F2S8-2%	0.2	0.8							2%
F2S8-4%	0.2	0.8							4%

*Steel fibers (length: 13mm and diameter: 200µm)

Lao, Jian-Cong, et al. *Composites Communications* 30 (2022): 101081.

Experimental Procedure

Samples casted into 50x50x50 mm^3 cubes and dumbbell samples ➡️ Demolding after 24hr curing under ambient temperature ➡️ Specimens sealed with plastic wraps subjected to 90°C for 72hrs ➡️ Samples stored in 23°C for 24hrs before the mechanical test
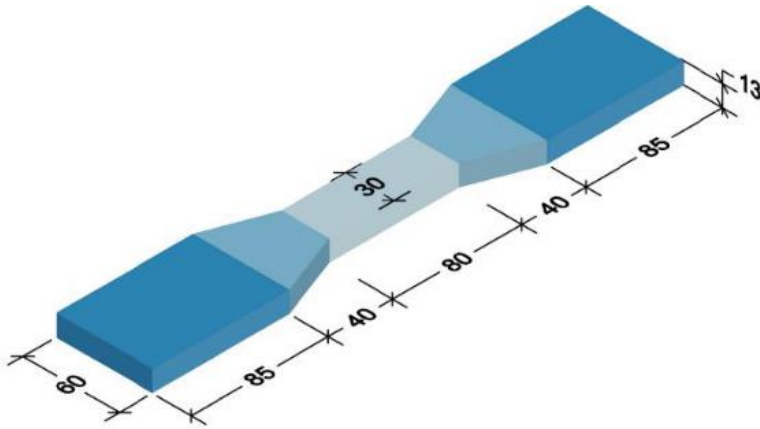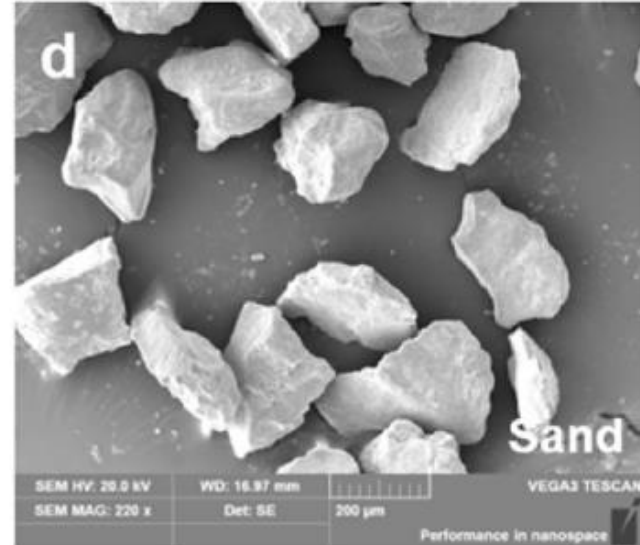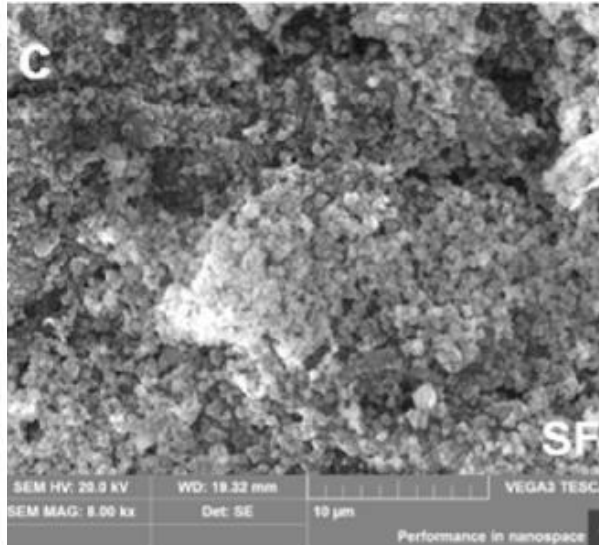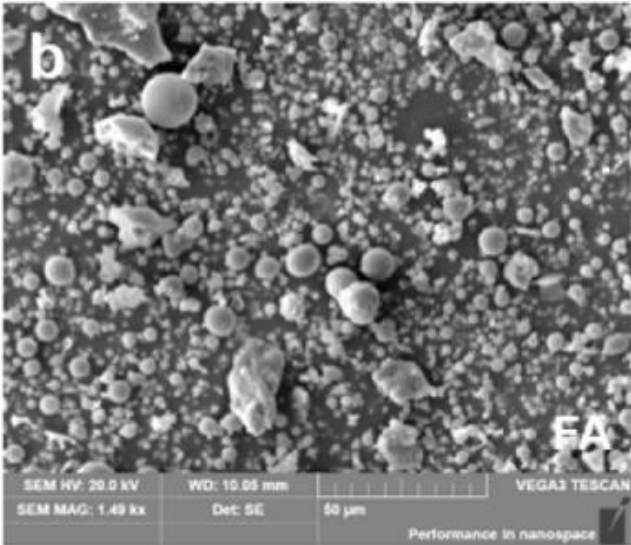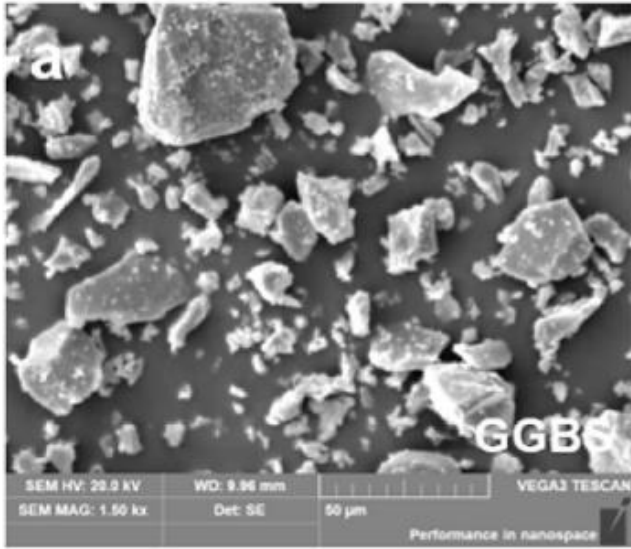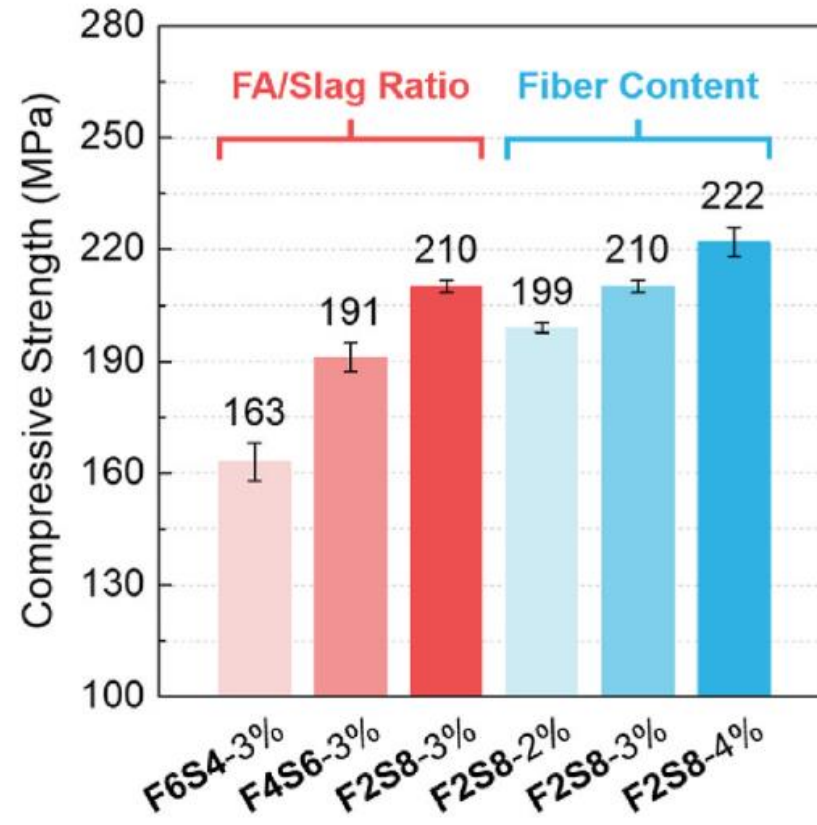

Unit: mm

Test	Loading rate
Compression strength	0.6 MPa/s
Tensile strength	0.5 mm/min

Lao, Jian-Cong, et al. *Composites Communications* 30 (2022): 101081.

Particle Size Distribution

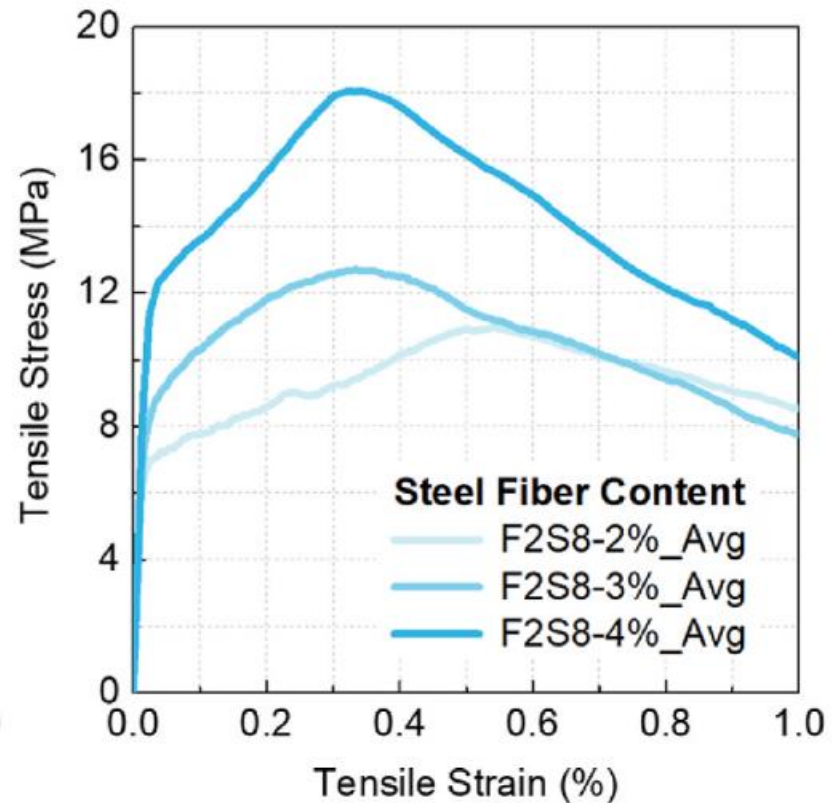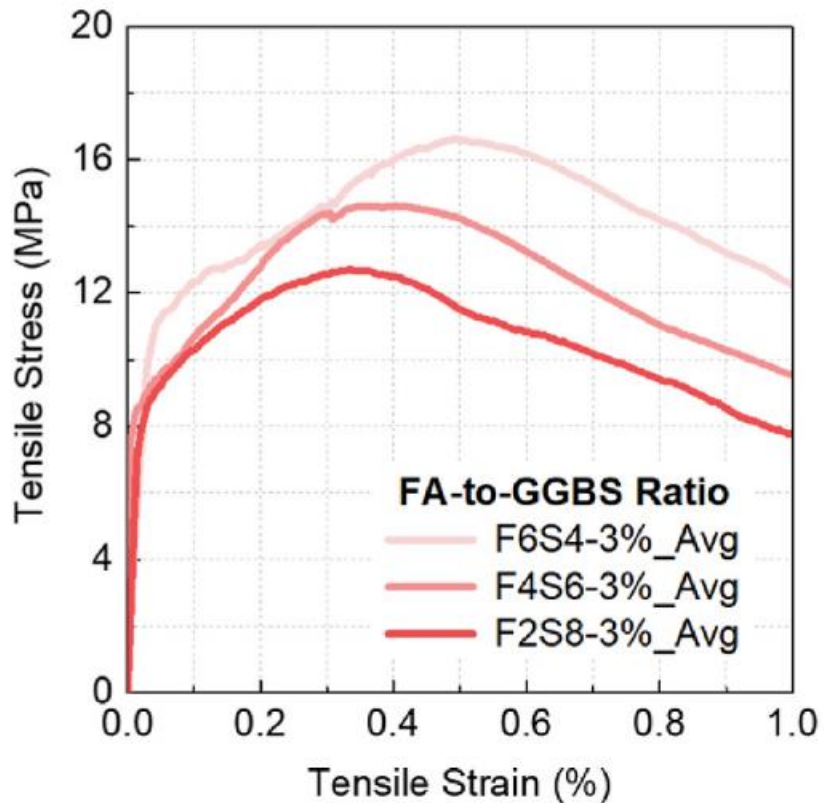Lao, Jian-Cong, et al. *Composites Communications* 30 (2022): 101081.
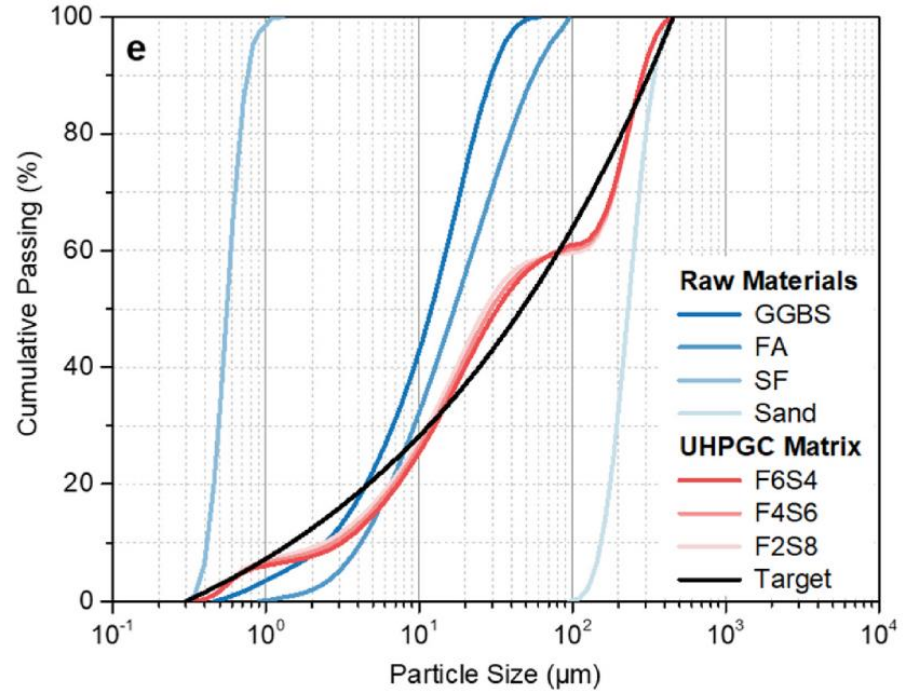
Compressive Strength comparison

- ✓ All mixes had compressive strength higher than 160 MPa.
- ✓ For UHPGC with different FA/GGBS ratios, FA/Slag of 0.25 had highest strength owing to higher alkali activation of GGBS than FA.
- ✓ Increase in compressive strength with increase in fiber content can be attributed to the strong modulus of steel fibers.

Lao, Jian-Cong, et al. *Composites Communications* 30 (2022): 101081.

UNIVERSITY OF TEXAS ★ ARLINGTON

Tensile test results

- ✓ Tensile strain capacity represents the strain corresponding to the peak stress in the stress-strain curve of UHPGC. The increase in slag content and steel fiber dosage both led to a reduced tensile strain capacity.
- ✓ Ultimate tensile strength was found to increase with the increase in fly ash content and increase in steel fiber content.
- ✓ An increase in strain hardening behavior was observed on increase in steel fiber content which was attributed to the increased fiber-bridging force generated from the higher steel fiber content.
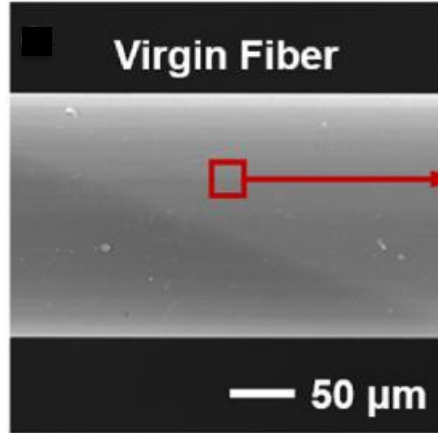
Lao, Jian-Cong, et al. *Composites Communications* 30 (2022): 101081.

Microscopic examination of UHPGC matrices
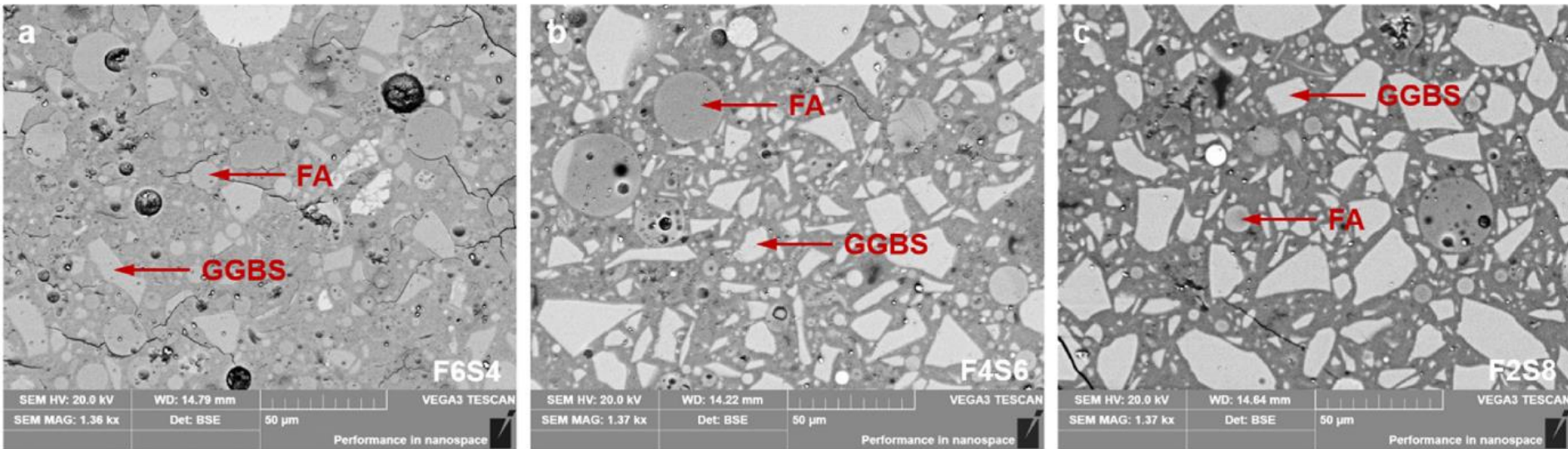
BSE images of matrices (a) F6S4 (b) F4S6 (c) F2S8

- ✓ A denser matrix with lower flaws was observed with an increase in slag content due to improved space-filling ability of the reaction product in the blended FA/GGBS system.
- ✓ Mix with higher fly ash content had more flaws which explains the lower UHPGC strength.

Lao, Jian-Cong, et al. *Composites Communications* 30 (2022): 101081.

UNIVERSITY OF TEXAS ⭐ ARLINGTON

EDS results of fiber surface at the fracture surface of F2S8-3%

Virgin Fiber

50 μm

Element	Composition (%)
Fe	61.9
Cu	19.7
Zn	10.3

Pull-out Fiber

50 μm
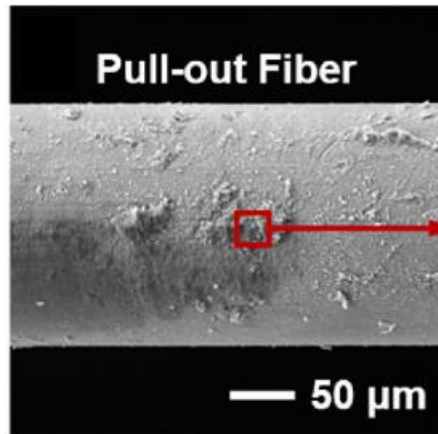
EDS analysis of the adhered
product was performed

Ca/Si = 0.35

Al/Si = 0.35

✓ Based on the Ca/Si and Al/Si ratios, the adhered product is C-(N)-A-S-H gel.
✓ Strong adhesive ability of C-(N)-A-S-H gel enhances the bond of steel fibers in the UHPGC matrix.

Lao, Jian-Cong, et al. *RILEM Strain Hardening Cementitious Composites - SHCC5 (2022)*

UNIVERSITY OF TEXAS ARLINGTON

UHPC with PE fibers

Precursor: Fly Ash, GGBS and Silica Fume
Activator: Sodium metasilicate and waterglass

Mix Proportions

Mix ID	Precursors			Fine Sand	Activators		Borax	Extra Water	Fiber
	FA	GGBS	SF		$Na_2SiO_3 -$ Anhydrous	Waterglass			
F8G2	847.2	211.8	55.7	334.4	105.8	157.6	31.7	196.4	2.0% (Vol) PE Fibers*
F5G5	539.1	539.1	56.7	340.5	107.7	160.5	32.3	200	
F2G8	219.6	878.6	57.8	346.8	109.7	163.5	32.9	203.7	

*PE fibers have a length of 18mm and a diameter of 24μm

Curing conditions:

Samples casted into specific molds covered with plastic sheet ➡ Demolding after 24hr sealed curing at ambient temperature ➡ Specim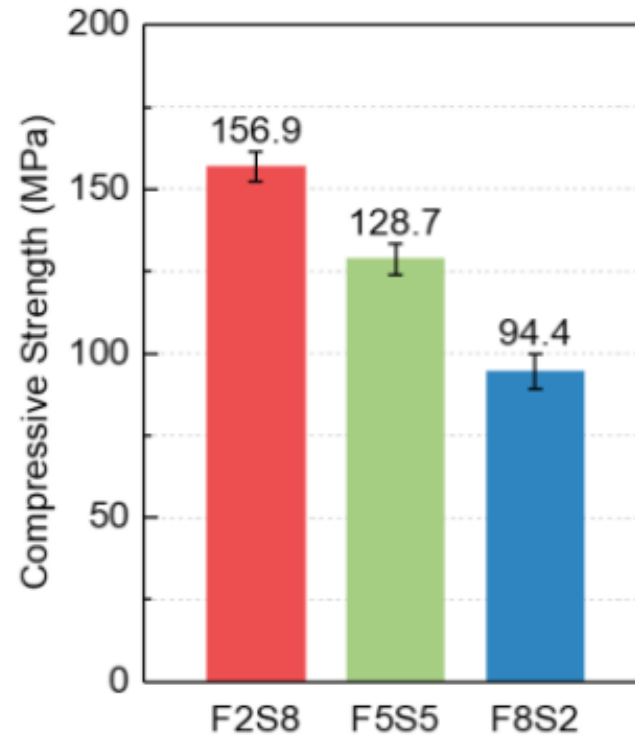ens sealed with plastic wraps subjected to 80°C for 72hrs ➡ After the heat curing, specimens taken out for mechanical testing

Lao, Jian-Cong, et al. *RILEM Strain Hardening Cementitious Composites - SHCC5 (2022)*

UNIVERSITY OF TEXAS ARLINGTON

Compressive Strength Results

Experimental Procedure: 50x50x50 mm^3 cubes subjected to a loading rate of 1.0MPa/s

Compressive strength increased with the decrease in FA/GGBS ratio due to the lower reactivity of FA compared to GGBS.

Lao, Jian-Cong, et al. *RILEM Strain Hardening Cementitious Composites - SHCC5 (2022)*

UNIVERSITY OF TEXAS ARLINGTON

Tensile Performance
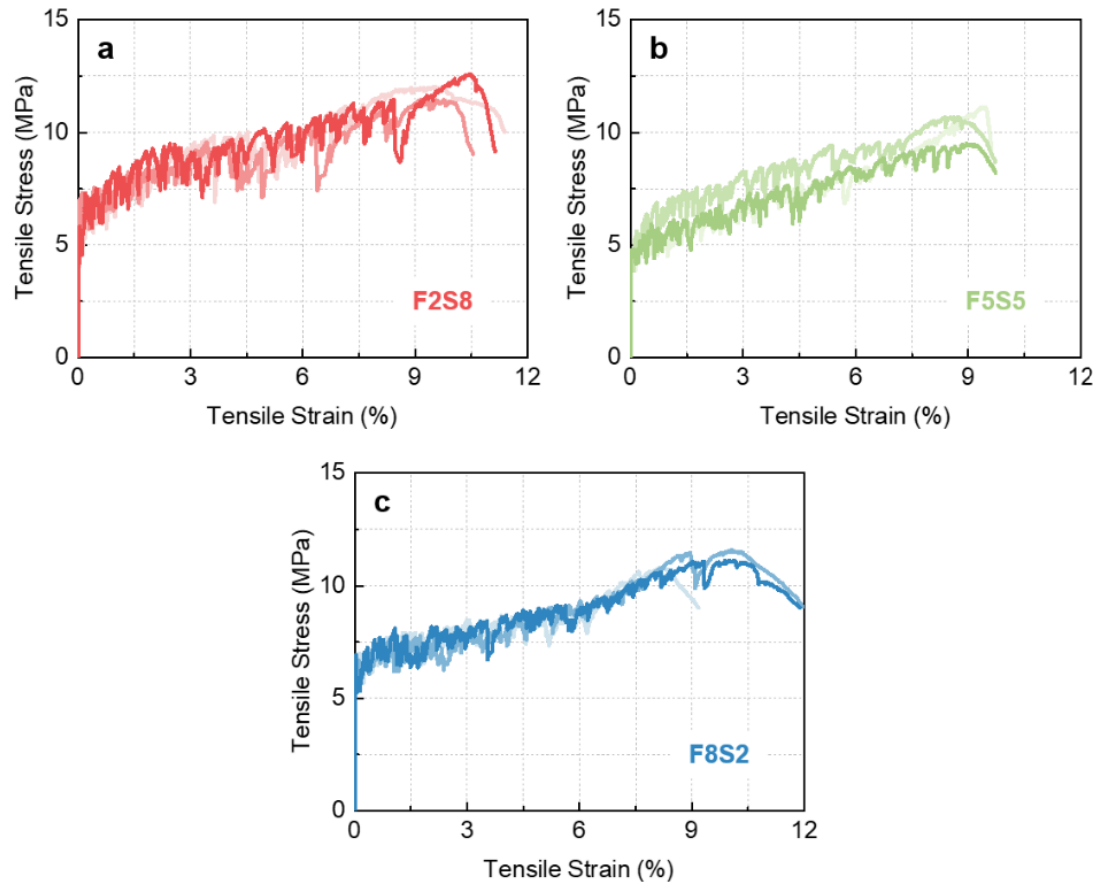
- ✓ Ultra-high tensile ductility (over 9.0%) was achieved for all mixes.
- ✓ FA/GGBS ratio had a marginal influence on the deformability.
- ✓ Larger stress drops were observed in mix F2S8 which indicates formation of cracks with larger widths. The mix F8S2 showed smaller stress drops.
- ✓ The use of higher FA/GGBS ratio resulted in more saturated cracks with narrowed widths.

BSE results of Matrix
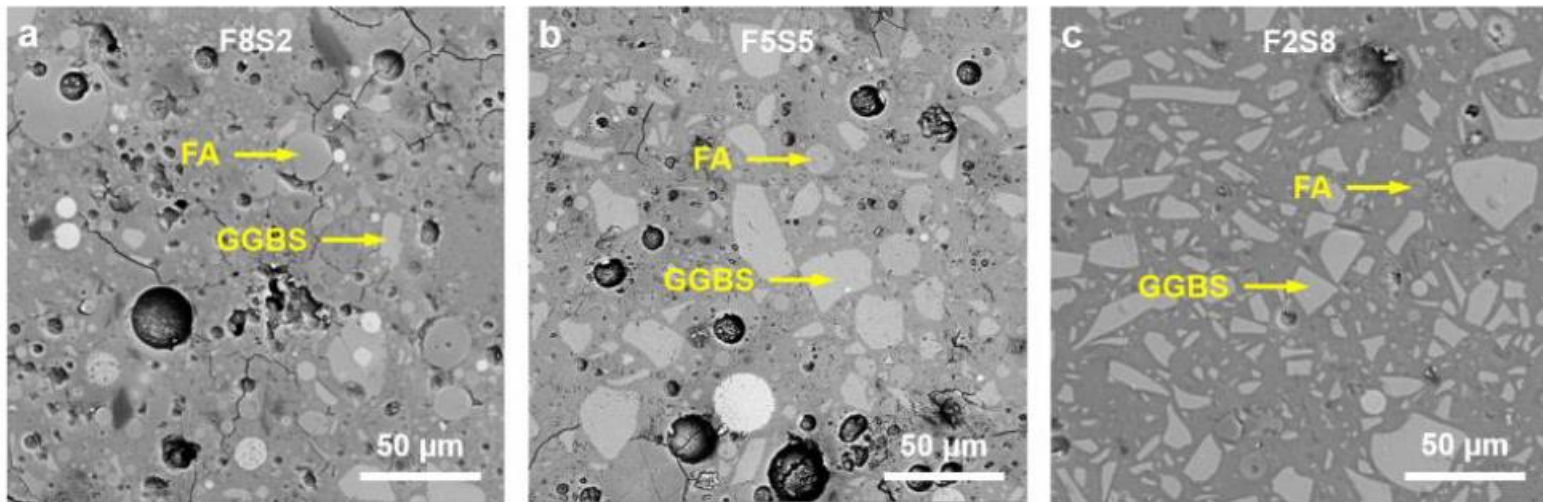
- ✓ Mix F8S2 with higher FA/GGBS ratio showed a looser paste microstructure with more heterogenous flaws compared to mix with F2S8.
- ✓ In the mix F5G5, denser microstructure is observed in locations with more unreacted GGBS particles.

This can be attributed to the N-A-S-H gel formed by the FA-based system which is less space filling than the C-(A)-S-H products generated from the activation of GGBS.

Lao, Jian-Cong, et al. *RILEM Strain Hardening Cementitious Composites - SHCC5 (2022)*

PE fibers reinforced UHPC with varying water to precursor ratio (w/p)

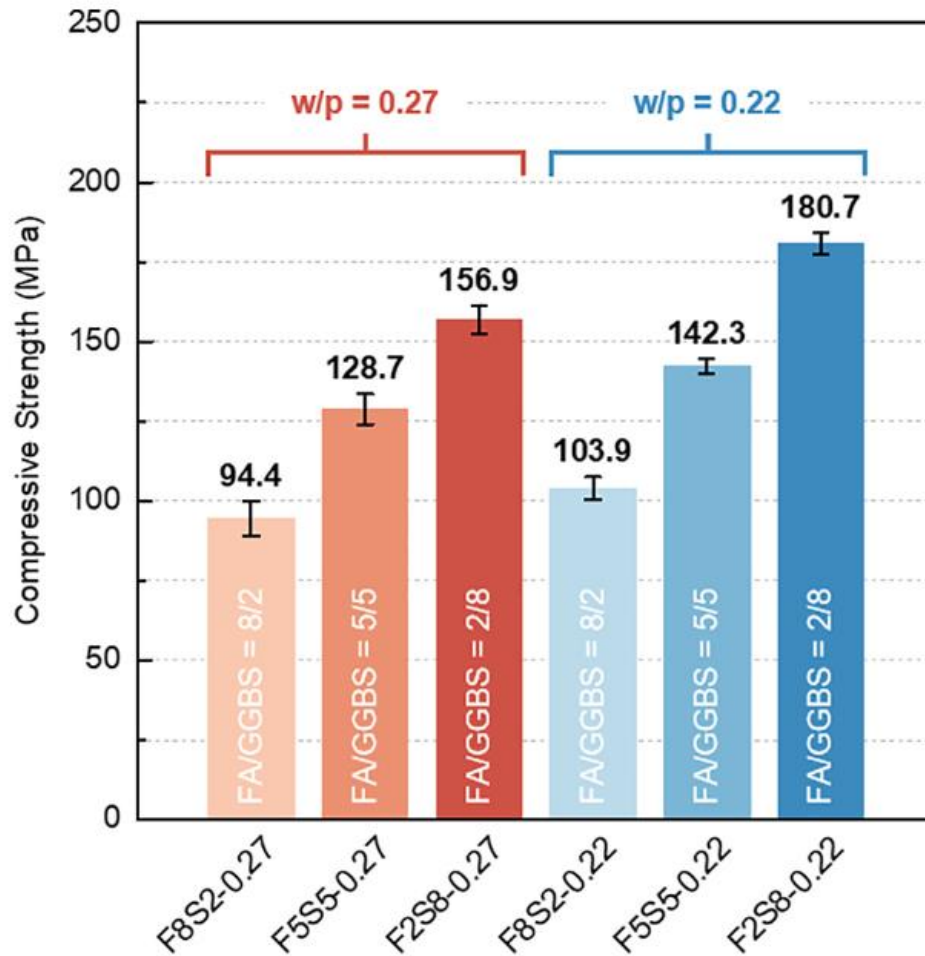**Precursor:** Fly Ash, GGBS and Silica Fume
Activator: Sodium metasilicate and waterglass

Mix Proportions

Mix ID	Precursors			Fine Sand	Activators		Borax	Extra Water	Total water	Fiber
	FA	GGBS	SF		Na_2SiO_3 – Anhydrous	Waterglass				
F8S2-0.22	0.760	0.190	0.050	0.030	0.095	0.141	0.038	0.122	0.220	2.0% (Vol) PE Fibers[*]
F5S5-0.22	0.475	0.475								
F2S8-0.22	0.190	0.760								
F8S2-0.27	0.760	0.190						0.172	0.270	
F5S5-0.27	0.475	0.475								
F2S8-0.27	0.190	0.760								

[*]Ultra-high-molecular-weight (UHMW) polyethylene (PE) fibers (length: 18mm, diameter: 24µm)

UNIVERSITY OF TEXAS ARLINGTON

Compressive Strength

Lao, Jian-Cong, et al. *Cement and Concrete Research 165 (2023): 107075.*
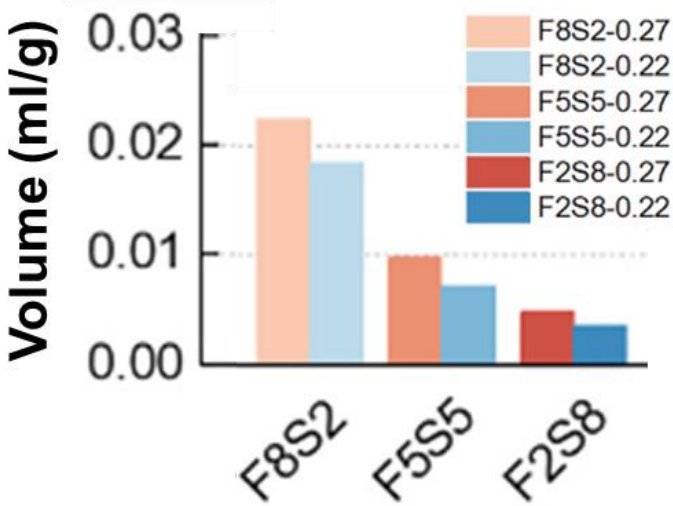
Bound water content
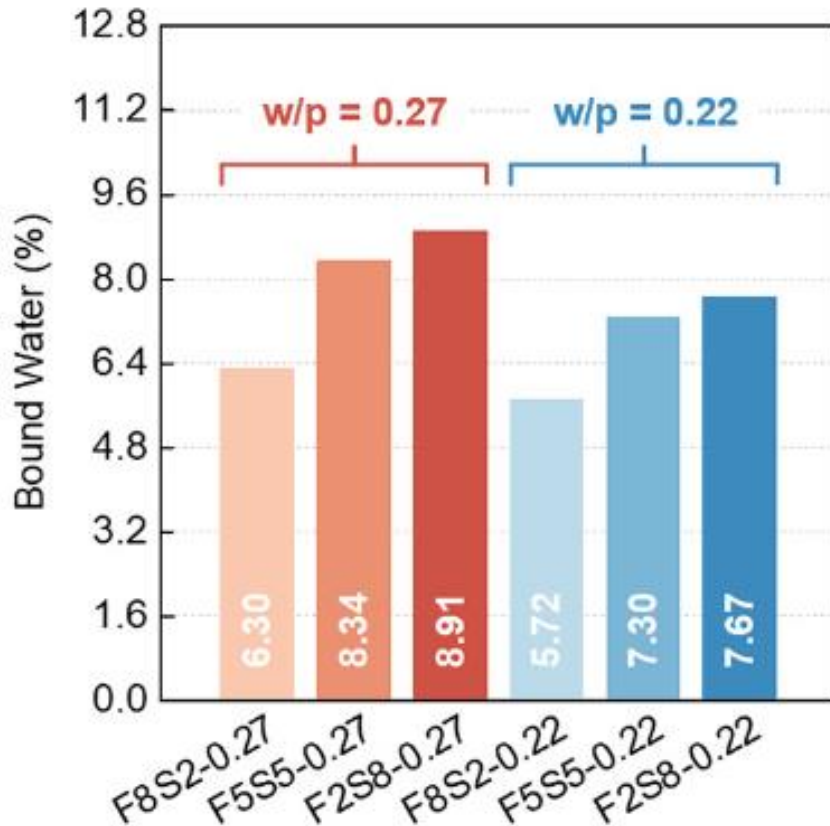
- ✓ Weight loss between 50°C and 550°C was measured for the bound water calculation.
- ✓ The main water binding component at this temperature range is C(N)ASH.

⬆ Slag content leads to ⬆ Bound water

⬆ Slag content causes ⬆ Ca/Si which ⬆ water binding ability of C(N)ASH

⬇ w/p content leads to ⬇ Bound water

Lao, Jian-Cong, et al. *Cement and Concrete Research 165 (2023): 107075.*

Capillary pore volumes
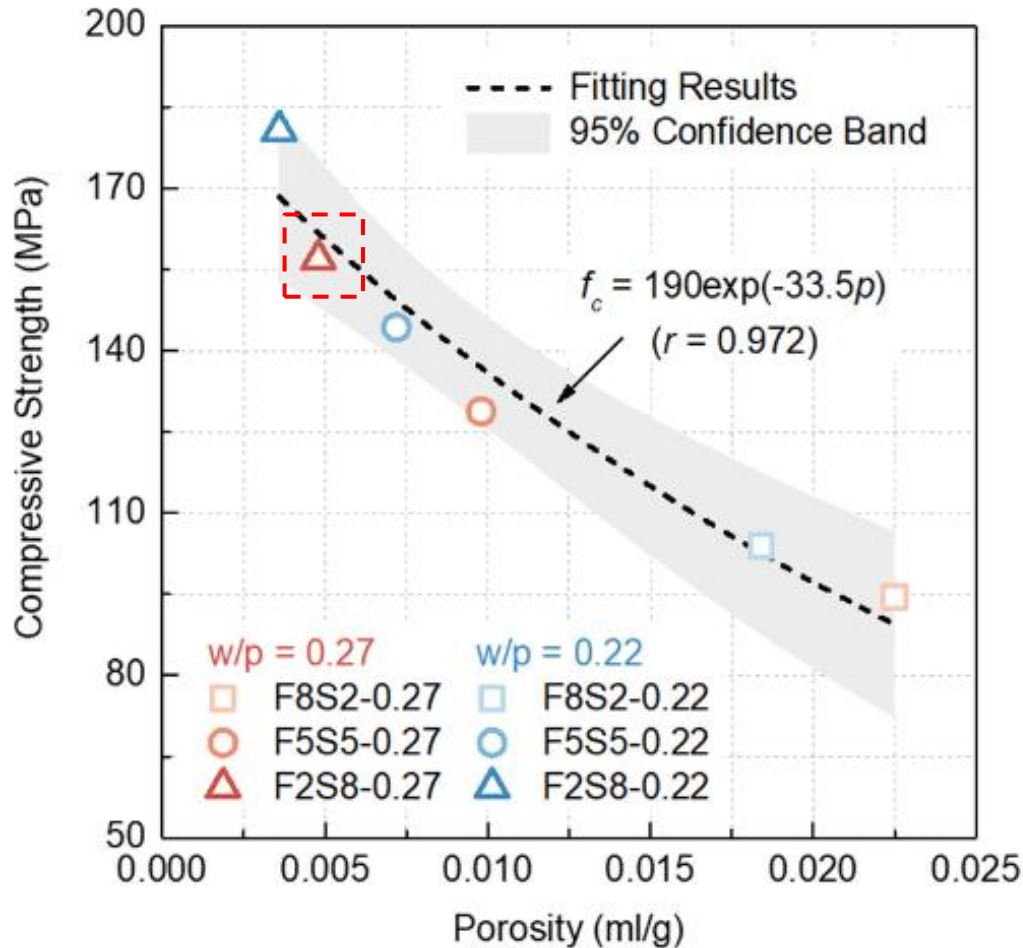

Brunauer–Emmett–Teller (BET) nitrogen adsorption

⬇ w/p content leads to denser matrix

⬆ Slag content leads to ⬇ capillary pore volume

⬆ Slag content causes ⬆ water binding ability of C(N)ASH which ⬇ the space left by unbound water.

Lao, Jian-Cong, et al. *Cement and Concrete Research 165 (2023): 107075.*

Relation between capillary porosity and compressive strength

Porosity strength relation:

$$f_c = f_0 e^{-kp}$$

Where,

f_c: Material strength
f_0: Strength when porosity is zero
k : constant
p : porosity

↓ w/p ratio leads to a denser microstructure

✓ F2S8-0.22 compressive strength close to theoretical strength when porosity is zero.
✓ Increasing slag content increases Ca/Si which leads to improved water binding ability resulting in fewer pores and higher compressive strength.

Lao, Jian-Cong, et al. *Cement and Concrete Research 165 (2023): 107075.*

UNIVERSITY OF TEXAS ⭐ ARLINGTON

Nano-indentation sample preparation

R_q = 26.6 nm

Topography (nm)

-100   -50   0   50   100
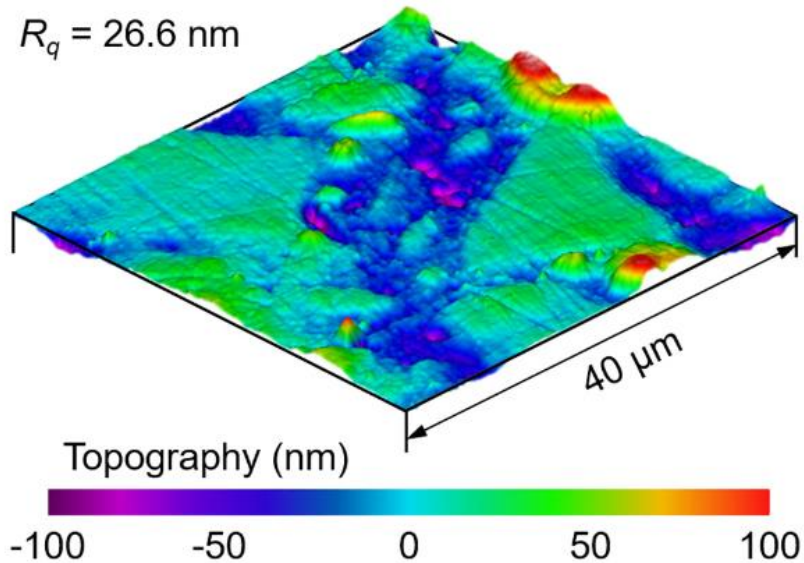
- ✓ RMS Roughness value calculated over 40x40 µm^2.
- ✓ Deconvolution of modulus distribution was performed to recognize the following phases:
  1. Low density (LD) C-S-H
  2. High density (HD) C-S-H
  3. Ultra high-density (UHD) C-S-H
  4. Unreacted FA and GGBS particles

40 µm

Experimental Procedure:

- ✓ Grid indentation was performed over 100x100 µm^2 grid with 10µm spacing.
- ✓ Load-indentation curves were generated by subjecting the sample to a linear load for 10 seconds, holding it at peak load (2000 µN) for 5 seconds, and then unloading it for 10 seconds.
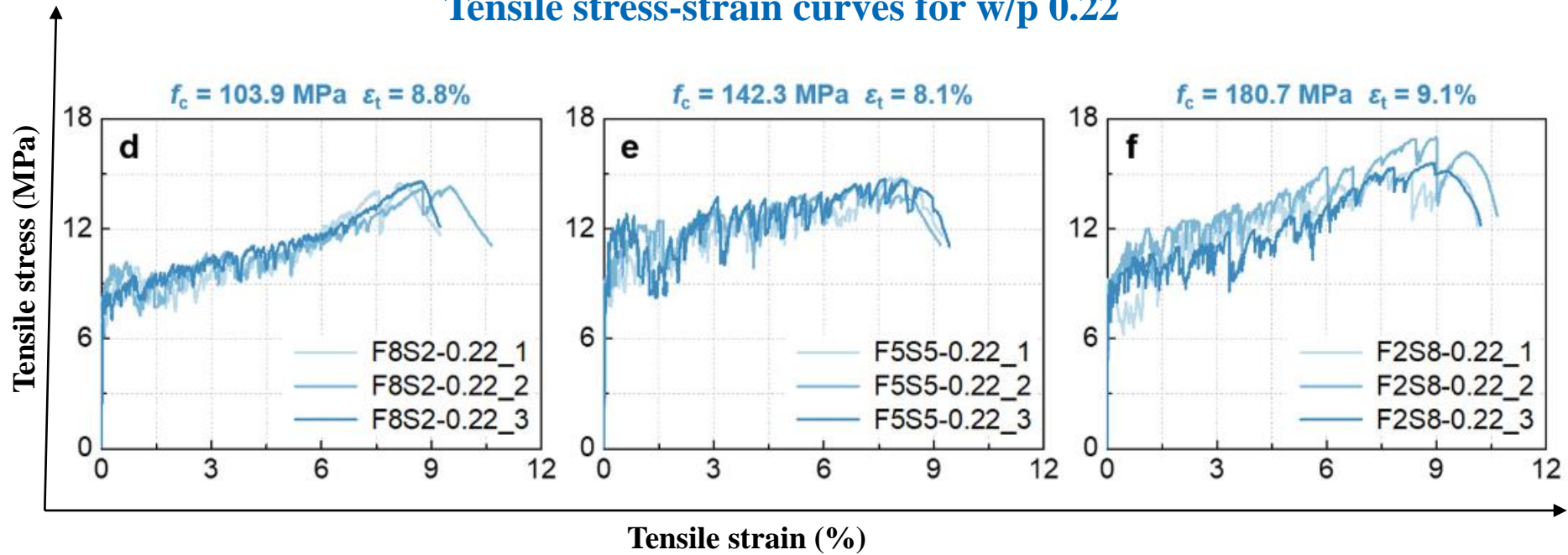
Probability density of elastic modulus for w/p 0.22
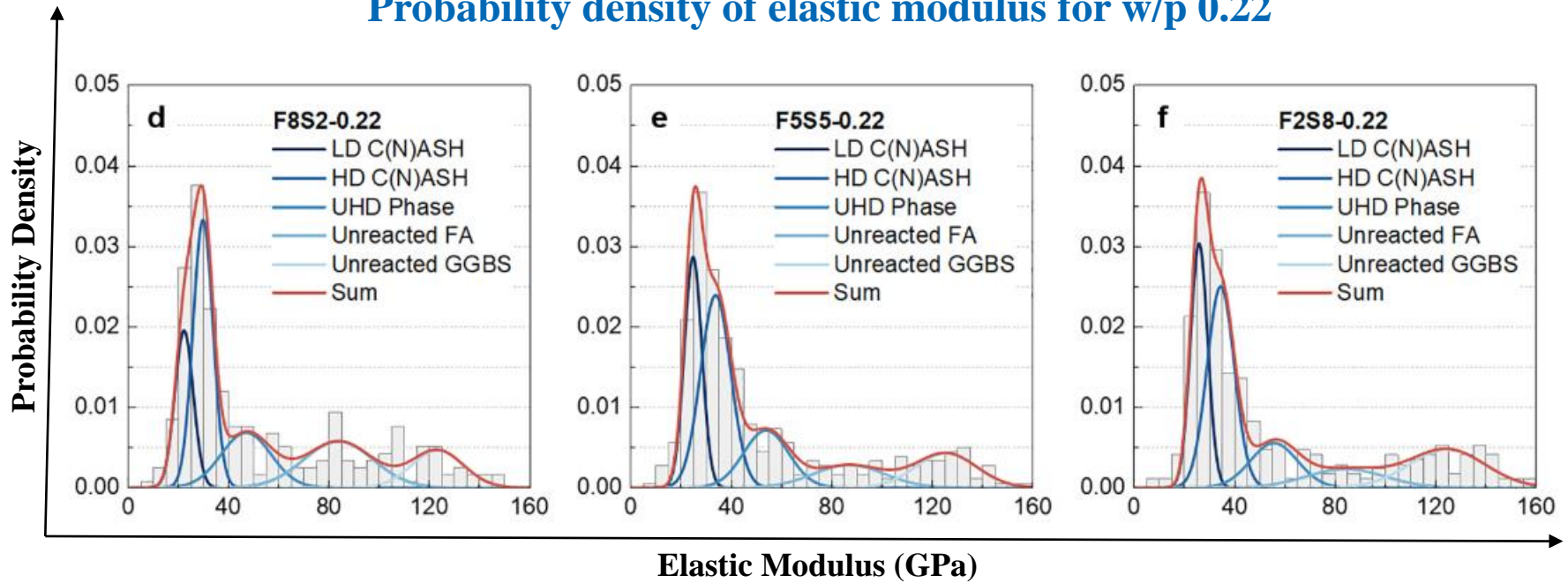
Average elastic modulus of single phase after deconvolution

Mix ID	LD C(N)ASH	HD C(N)ASH	UHD Phase	Unreacted particles	
				FA	GGBS
F8S2-0.22	22.2±3.7	29.8±4	47±9.9	83.8±13.8	123.3±10.3
F5S5-0.22	24.8±3.5	33.8±6	53.9±9	86.8±14.2	125.6±12.2
F2S8-0.22	25.9±3.4	34.5±5.4	55.7±9.4	84.2±15.6	124.6±15.1

LD: low density, HD: high density, UHD: ultra-high density

UNIVERSITY OF TEXAS ARLINGTON

Tensile stress-strain curves for w/p 0.22

$f_c = 103.9$ MPa $\varepsilon_t = 8.8\%$ $f_c = 142.3$ MPa $\varepsilon_t = 8.1\%$ $f_c = 180.7$ MPa $\varepsilon_t = 9.1\%$

- ✓ All mixes displayed pronounced strain hardening behavior with a tensile strain capacity of over 8%.
- ✓ **F2S8 displayed highest compressive strength, tensile strength and tensile strain capacity**

Lao, Jian-Cong, et al. *Cement and Concrete Research 165 (2023): 107075.*

UNIVERSITY OF TEXAS ARLINGTON

Summary of mechanical properties

| Mechanical properties	F8S2-0.22	F5S5-0.22	F2S8-0.22
Ultimate tensile strength (MPa)	14.5 ± 0.2	14.4 ± 0.6	15.9 ± 1.0
Tensile strain capacity (%)	8.8 ± 0.7	8.1 ± 0.1	9.1 ± 0.3
Average crack width at the ultimate tensile strain (µm)	76.8 ± 7.5	125.3 ± 11.9	109.0 ± 11.3

UNIVERSITY OF TEXAS ARLINGTON

DIC strain fields at different tensile strain levels (3.0%, 6.0% and ultimate strain)

✓ Cracking behavior visualized by strain field analyzed by DIC technique.
✓ **Saturated multiple cracking observed.**

Average crack width is between 110-130μm < **Maximum allowable crack width for concrete members subjected to extreme environments (0.33 mm – ACI 318)**

F2S8

80mm

$\varepsilon = 3.0\%$ $\varepsilon = 6.0\%$ $\varepsilon = 8.9\%$ **(Ultimate strain)**

Lao, Jian-Cong, et al. *Cement and Concrete Research 165 (2023): 107075.*
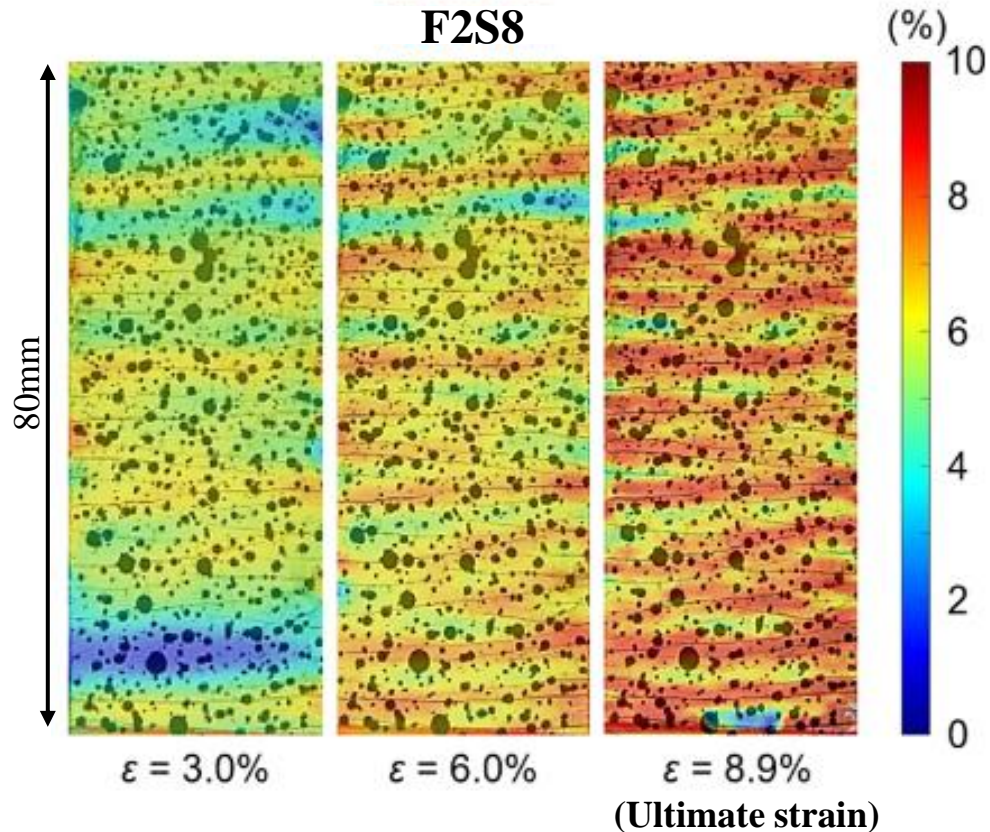
Compressive strength vs tensile strain capacity relations

Comparison between existing literature and proposed mix in this study
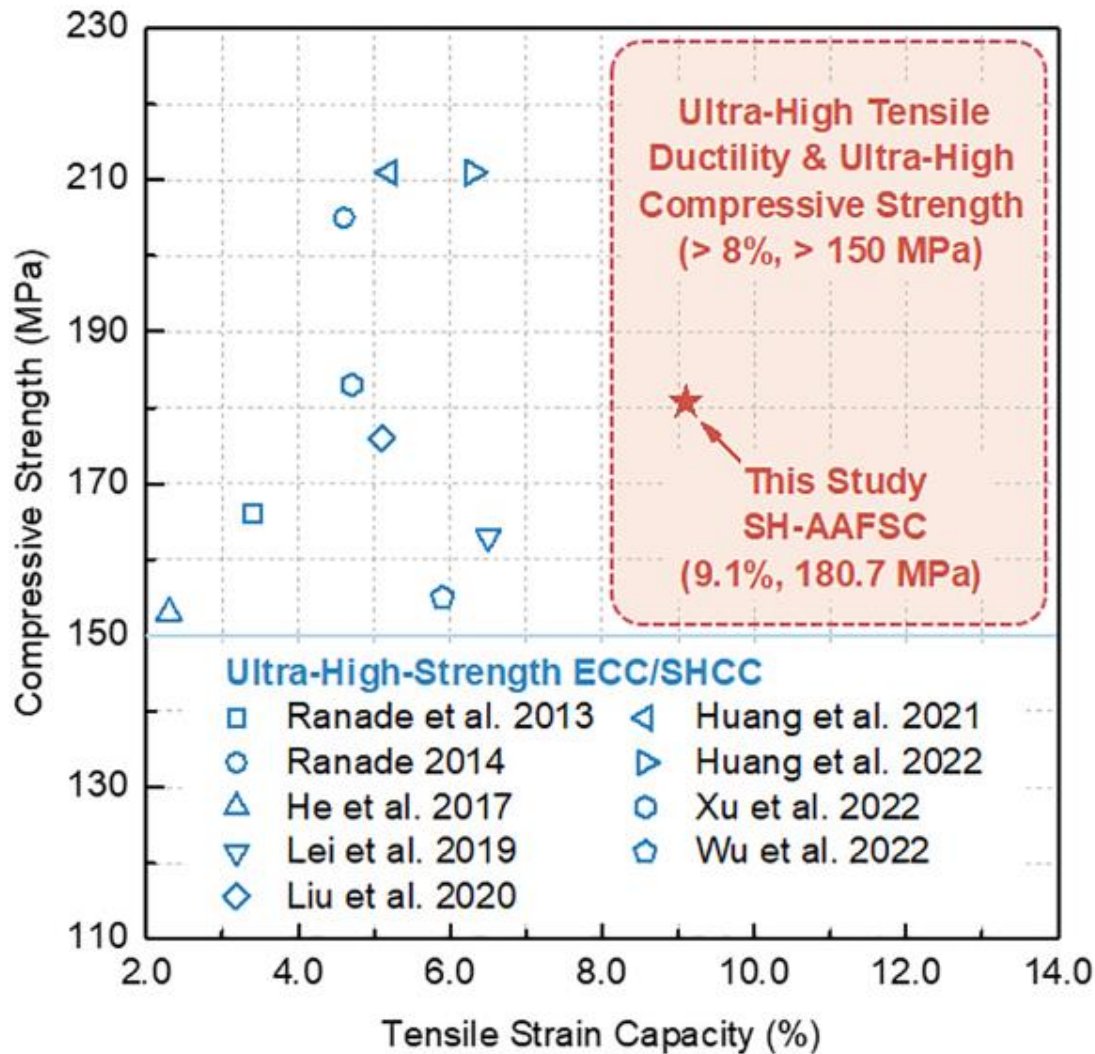
- ✓ **Simultaneously achieved ultra-high compressive strength and ultra-high tensile ductility.**
- ✓ Mix developed in this study showed compressive strength between 94.4-180.7MPa and a tensile strain capacity of 8.1-9.9%.

Lao, Jian-Cong, et al. *Cement and Concrete Research 165 (2023): 107075.*

UNIVERSITY OF TEXAS ARLINGTON

Center for Advanced Construction Materials

Thank you!